ELSEVIER

Cement and Concrete Research

Editor: Karen Scrivener
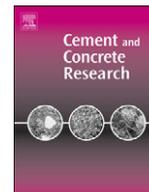
Influence of particle size distributions on yield stress and viscosity of cement–fly ash pastes

Dale P. Bentz [a],*, Chiara F. Ferraris [a], Michael A. Galler [a], Andrew S. Hansen [b], John M. Guynn [b]

[a] Building and Fire Research Laboratory, National Institute of Standards and Technology, 100 Bureau Drive Stop 8615, Gaithersburg, MD 20899, United States
[b] Roman Cement LLC, United States

ARTICLE INFO

ABSTRACT

The rheological properties of blended cement-based materials depend strongly on mixture proportions and the characteristics of the components. In this study, design of experiments is used to investigate the influence of three variables (cement particle size distribution (PSD), fly ash PSD, and ratio of fly ash to cement) at each of four levels on the yield stress and viscosity of blended pastes. Both rheological parameters are seen to vary over several orders of magnitude for the evaluated design space. Physical characteristics of the powders, such as cement and total particle densities and total particle surface area, are computed for each mixture. A percolation-type relationship is observed between yield stress and cement particle (number) density. While neither apparent nor plastic viscosities were particularly well described by the commonly employed Kreiger–Dougherty equation, plastic viscosities were found to be linear functions of either total (cement + fly ash) particle surface area or total particle density.

Published by Elsevier Ltd.

1. Introduction

The rheological properties of cement paste are critical to the field performance of concrete in terms of its slump, flow, and workability [1]. The rheology of cement paste is strongly influenced by mixture proportions and material characteristics, including water-to-cementitious materials ratio by mass (w/cm), supplementary cementitious material (SCM) additions, and the fineness of the powder materials. The current study focuses on the latter two of these parameters, while maintaining a constant volume fraction of water in all investigated mixtures. While Papo et al. [2] have noted that "higher surface area corresponds to a higher water adsorption and higher interparticle interactions, resulting in higher viscosity of the paste at the same solid content," there exist few if any quantitative studies examining the influence of particle size distribution (PSD) on the yield stress and viscosity of (blended) cement pastes. Lee et al. [3] have noted that as the PSD of a cement/fly ash paste becomes wider, paste fluidity increases (apparent viscosity decreases). In the present paper, the relationship between the rheological parameters of yield stress and viscosity and characteristics of the cement/fly ash PSD including particle density and surface area will be examined. These rheological studies transcend the field of cement-based materials, as rheology is critical to a wide variety of practical systems including

the flow of magma [4,5], the processing and taste of chocolate [6,7], and the emerging field of nanocomposites [8,9].

2. Materials and experimental procedures

A commercially available Type I/II (ASTM C150 [10]) cement and a Class F fly ash (ASTM C618 [11]) were obtained from their respective manufacturers. The cement has a Blaine fineness of 376 m^2/kg and a potential Bogue phase composition of 57% C$_3$S, 15% C$_2$S, 7% C$_3$A, and 10% C$_4$AF by mass. Its measured density is 3200 kg/m^3 ± 10 kg/m^3 (ASTM C188 [12]). According to the manufacturer, the Class F fly ash contains major oxides of 52.9% SiO$_2$, 26.4% Al$_2$O$_3$, 8.5% Fe$_2$O$_3$, and 2.1% CaO by mass, with measured strength activity indices [13] of 88% and 92% at 7 d and 28 d, respectively. Its density is reported by its manufacturer as 2300 kg/m^3. Four additional cements were produced by processing the original cement to achieve four distinct D$_{90}$ values by mass for their PSDs as measured by laser diffraction (nominally 24 μm, 12 μm, 11 μm, and 9 μm in comparison to the D$_{90}$ of 36 μm for the original cement). The value of D$_{90}$ is the size of the particle for which 90% of the sample by mass is below this size. Additionally, the fly ash was processed to produce four additional fly ashes with different D$_{10}$ values for their PSDs (nominally 4 μm, 11 μm, 13 μm, and 15 μm vs. 2.7 μm for the original fly ash). The PSDs of the five cements and the five fly ashes as measured using laser diffraction techniques with isopropanol as the solvent are provided in Figs. 1 and 2 for the cements and fly ashes, respectively. Assuming spherical particles and utilizing the measured densities for the various powders, these PSDs were analyzed to determine surface areas per unit mass and particle number densities per unit volume for
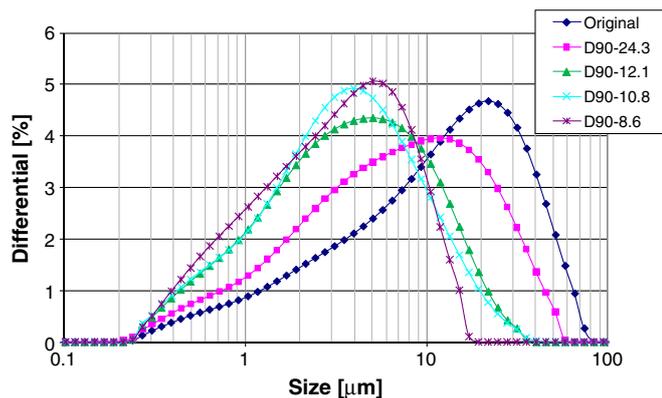
Fig. 1. Particle size distributions of the five cements. Each shown result is the average of six individual measurements and the error bars (one standard deviation) would fall within the size of the shown symbols.

Table 1
Computed PSD characteristics of cements and fly ashes.

Component	Specific surface area (m^2/kg)	Particle density $(\#/100 \, \mu m^3 \text{ solids})$
Original cement	485	102.3
$D_{90} = 24.3 \, \mu m$ cement	670	169.2
$D_{90} = 12.1 \, \mu m$ cement	964	230.6
$D_{90} = 10.8 \, \mu m$ cement	1017	244.4
$D_{90} = 8.6 \, \mu m$ cement	1096	257.6
Original fly ash	432	30.7
$D_{10} = 4.2 \, \mu m$ fly ash	379	31.5
$D_{10} = 10.8 \, \mu m$ fly ash	114	0.048
$D_{10} = 13.0 \, \mu m$ fly ash	96	0.027
$D_{10} = 14.8 \, \mu m$ fly ash	103	0.017

each powder material, as indicated in Table 1. The particle densities for the three coarsest fly ashes are several orders of magnitude smaller than those of the other two fly ashes, due to their absence of fly ash particles smaller than 5 μm.

To directly examine the influence of mixture proportions (cement/fly ash volumetric ratio) and PSDs on performance, all pastes were prepared at a constant volumetric water-to-solids ratio. To avoid introducing an additional variable, high range water reducing agents were not employed in any of the pastes. The control mixture was a paste prepared with the original cement with a conventional water-to-cement ratio (w/c) of 0.35 by mass. This is equivalent to a water volume fraction of 0.528, ignoring any air entrainment by the paste. Seventeen subsequent mixtures were prepared maintaining this volume fraction of water, while varying the cement PSD, the fly ash PSD, and the proportion of cement to fly ash. Thus, the mass-based water-to-cementitious materials ratio (w/cm) of each mixture was different. Each of these three variables was set at four levels, with the volume percentages of fly ash in the cement/fly ash blends being investigated at levels of 20%, 35%, 50%, and 65%. The total experimental space of $64 = 4^3$ mixtures was reduced to 16 using a fractional factorial experimental design [14]. The order of these mixtures was then randomized. An additional control mixture of a 50:50 volumetric mixture of the original cement and original fly ash was also investigated. Table 2 provides the details on the mixtures in their order of execution.

All cement pastes were prepared in a high shear blender following the procedure developed by the Portland Cement Association [15] and described in detail in Sant et al. [16]. For a given mixture, all
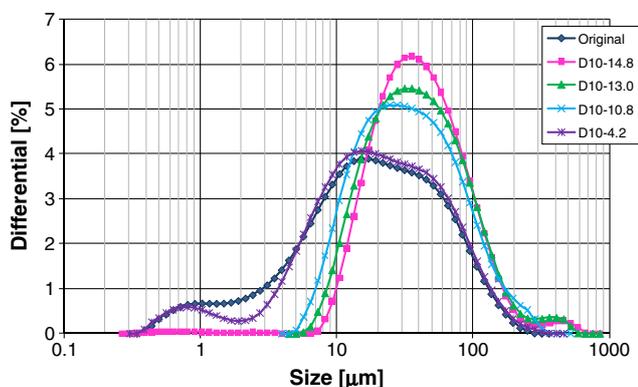
powder materials were first pre-blended for 30 min in a sealed plastic jar in a Turbula [1]three-dimensional mixer that allows a material contained in a jar to be tumbled and rolled at the same time. No water reducer was employed in any of the pastes. Immediately following mixing, small specimens were obtained for rheology measurements. The rheological properties of mixture #9, with the highest total particle surface area and highest cement particle density, could not be measured due to the extreme stiffness of its paste.

Rheological properties of the prepared cement pastes were measured using a rotational rheometer [17,18]. The configuration employed parallel plates with serrated surfaces. The plates had a diameter of 35 mm, with a gap of 0.4 mm. For the measurement loop, the shear rate ranged from $0 \, s^{-1}$ to $50 \, s^{-1}$, as determined by analytical calculation from the rotational speed [19]. To first homogenize the specimen, an increasing shear rate up to $70 \, s^{-1}$ was imposed for 200 s, before executing the loop of increasing and then decreasing the shear rate. The induced shear stresses were measured, corresponding to 10 shear rates when increasing the rotational velocity, and 10 further levels when decreasing the rotational velocity. Based on the procedures developed in a previous study [20], each measured point was recorded after the shear stress reached equilibrium or after 20 s, whichever occurred first. A typical shear stress vs. shear rate curve for the descending data is provided in Fig. 3. These descending curve data were fitted to a linear equation using ordinary least squares regression to determine a slope (plastic viscosity) and an intercept (yield stress), according to a Bingham model as shown in Eq. (1):

$$\tau = \tau_0 + \eta \dot{\gamma} \tag{1}$$

where τ is the measured shear stress at a shear rate of $\dot{\gamma}$, τ_0 is the yield stress, and η is the plastic viscosity. By comparison, the apparent viscosity, η_a, is typically reported as the ratio of the measured shear stress to the applied shear rate ($\tau/\dot{\gamma}$) at a specific shear rate [17]. Replicate measurements on three separately prepared samples of cement paste indicated coefficients of variation of 20% and 15% for yield stress and plastic viscosity, respectively.

To examine the variation in maximum packing fraction with PSDs, a subset of the prepared pastes was centrifuged at 800 g for 20 min at 25 °C [7]. The maximum packing fraction was computed as the ratio of the total volume of solids introduced into the cylindrical sample holder to the volume of the sediment bed after centrifuging. In addition, particle packing simulations using spherical particles were conducted using previously developed software [21] to provide a second estimate of these maximum (random) packing fractions. The PSDs

Fig. 2. Particle size distributions of the five fly ashes. Each shown result is the average of six individual measurements and the error bars (one standard deviation) would fall within the size of the shown symbols.

Table 2
Cement–fly ash mixtures in order of execution.

Mixture	Cement	Fly ash	Fly ash volume percentage
1	Original ($D_{90} = 36$)	None	0%
2	Original ($D_{90} = 36$)	Original ($D_{10} = 2.7$)	50%
3	$D_{90} = 24$	$D_{10} = 13$	35%
4	$D_{90} = 24$	$D_{10} = 15$	50%
5	$D_{90} = 12$	$D_{10} = 15$	35%
6	$D_{90} = 11$	$D_{10} = 11$	50%
7	$D_{90} = 9$	$D_{10} = 15$	65%
8	$D_{90} = 11$	$D_{10} = 4$	35%
9	$D_{90} = 9$	$D_{10} = 4$	20%
10	$D_{90} = 9$	$D_{10} = 11$	35%
11	$D_{90} = 12$	$D_{10} = 11$	65%
12	$D_{90} = 9$	$D_{10} = 13$	50%
13	$D_{90} = 24$	$D_{10} = 11$	20%
14	$D_{90} = 12$	$D_{10} = 13$	20%
15	$D_{90} = 24$	$D_{10} = 4$	65%
16	$D_{90} = 12$	$D_{10} = 4$	50%
17	$D_{90} = 11$	$D_{10} = 15$	20%
18	$D_{90} = 11$	$D_{10} = 13$	65%

obtained for each mixture by combining the measured PSDs of the two (cement and fly ash) starting powders were employed as inputs to these simulations.

3. Results and discussion

The rheological parameters, namely yield stress and plastic viscosity, were calculated from the measured shear stress-shear rate curves for each of the mixtures in Table 2 by linear regression. The correlation coefficients (R^2) for these regressions ranged between 0.89 and 1.00, with an average value of 0.96 and a standard deviation of 0.04. The calculated yield stresses and plastic viscosities are provided in Table 3. Each of the two parameters ranged over about two orders of magnitude, indicating the strong influence of PSD on rheological properties. Separate detailed discussions for yield stress and viscosity follow.

3.1. Yield stress

It is generally accepted that in the absence of chemical admixtures, cement pastes will strongly flocculate [22,23]. Breaking down this flocculated structure into smaller flocs or individual particles to induce flow requires the application of a finite (yield) stress. As these interparticle force bonds are replaced and augmented by "cement hydration product" bonds, this yield stress increases over time, until ultimately a rigid viscoelastic solid is produced (cement paste's setting process) [16,23]. In this study, measurements were made during the induction period of cement hydration, so that the yield stress is dominated by the initial interparticle forces present in
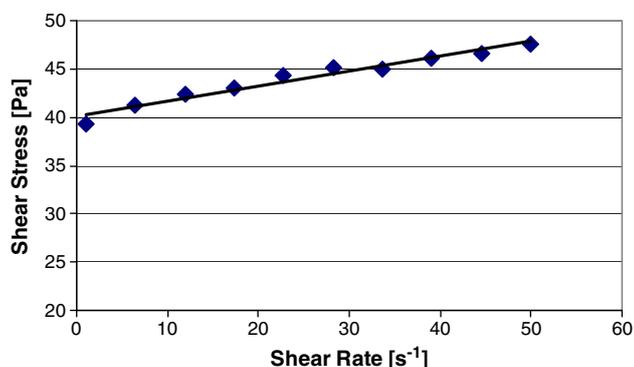

Fig. 3. Typical descending branch shear stress vs. shear rate curve obtained for a cement/fly ash paste mixture.

Table 3
Yield stress and plastic viscosity determined for each blended cement paste mixture at a solids volume fraction of 0.472.

Mixture	Mixture total surface area (m^2/cm^3 solids)	Cement particle density (#/100 μm^3 solids)	Yield stress (Pa)	Plastic viscosity (Pa·s)	Maximum packing fraction
1	1.55	102.3	2.84	0.21	0.54
2	1.27	51.2	1.03	0.050	0.58
3	1.51	110.0	22.9	0.27	0.54
4	1.22	84.6	6.8	0.15	0.58
5	2.13	149.9	336	2.3	0.52
6	1.77	122.2	108	0.62	0.55
7	1.39	90.2	30.1	0.15	0.58
8	2.43	158.8	288	1.4	0.52
9	3.00	206.1	Not measurable	Not measurable	Not measured
10	2.38	167.4	132	0.65	0.50
11	1.27	80.7	5.59	0.10	0.58
12	1.87	128.8	66.5	0.32	0.55
13	1.82	135.4	37.5	0.31	0.53
14	2.56	184.5	403	1.5	0.51
15	1.34	59.2	2.88	0.091	0.58
16	2.01	115.3	65.6	0.58	0.54
17	2.67	195.5	534	2.6	0.51
18	1.29	85.5	22.2	0.091	0.57

each mixture. For the analysis to follow, it is assumed that while strong interparticle forces exist between two cement particles, in comparison, those between two fly ash particles and between a fly ash and a cement particle are negligible. Two justifications for this, obtained in this study, were as follows. First, the best fits to the experimental data were obtained employing this assumption. Second, a paste prepared with only the original fly ash and a water volume fraction of 0.528 exhibited excessive settlement and bleeding, indicating a very low or zero yield stress value. However, it would be quite useful to directly measure the interparticle forces between these different powder components of the blended cement pastes in the future.

Practically, the results in Table 3, all obtained at a constant solids (particle) volume fraction of 0.472, indicate that the replacement of cement by fly ash will decrease the yield stress, as it proportionally decreases the cement particle density and therefore reduces the number of flocculated cement particle to cement particle connections (dilution effect as opposed to a ball-bearing effect [24]). This is in agreement with general observations of the effects of fly ash on rheology of cement-based materials [1], although often the fly ash replacement is performed on a mass basis at a constant mass fraction of solids (constant w/cm), thereby confounding the change in cement particle density with a change (typically an increase) in overall solids volume fraction. Similar observations have been made in other materials, including dispersions of sugar crystals in chocolate, where increasing particle size at a constant volume fraction (thus decreasing particle density) produced significantly lower values for yield stress [6]. Chocolate is an interesting analogy for cement-based materials, as the particle sizes are in the same range, nominally 1 μm to 100 μm, for both systems.

The yield stress behavior of the 17 paste mixtures was further analyzed using a percolation approach [4,5,9] in which a power law proportionality is assumed between the cement particle density, φ, and the measured yield stress, τ_0:

$$\tau_0 \alpha (\varphi - \varphi_c)^\beta \tag{2}$$

with β being the critical percolation exponent for yield stress and α indicating proportionality. In the present study, various values for the percolation threshold parameter, φ_c, were examined, but the best fit was provided with a value of $\varphi_c = 0$, suggesting that very few cement particles are required to form a percolating network
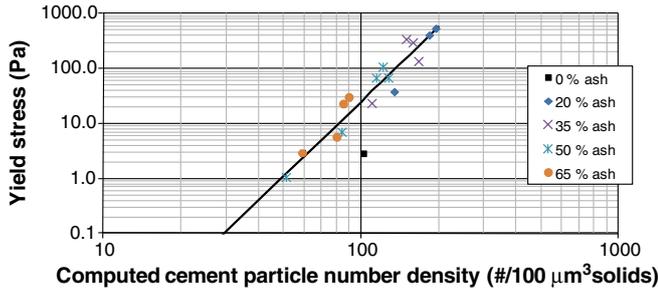
Fig. 4. Log–log plot of yield stress vs. cement particle density. Best fit ($R^2 = 0.918$) is shown for all of the data with the exception of the single 0% fly ash data point.

structure, likely due to their strong tendency to flocculate. A log–log plot of the data is provided in Fig. 4, with the best fit line having a slope, $\beta = 4.5 \pm 0.4$. This value is in the range of those determined in other multi-phase systems. For example, Loiseau and Tassin [9] analyzed the rheology of laponite-polyethylene oxide nanocomposites and determined percolation exponents of 3.3 and 4.5 for yield stress and elastic modulus, respectively. Walsh and Saar [4] determined critical exponents for yield stress of crystal networks in magma that increased from 3.6 to 4.6 as the air bubble content of the magma increased from 0 to 0.5. In the present study, as shown by the four sets of data points in Fig. 4, the determined slope was independent of the fly ash volume fraction. This suggests that in each random cement/fly ash particle configuration, the cement particles are able to arrange themselves in a consistent manner regardless of the (occluded) volume occupied by the far fewer number of fly ash particles, since the fly ash particles are in general larger than the cement particles. This was not the case in the simulated magma–air systems of Walsh and Saar [4,5], where the presence of the air bubbles significantly modified the spatial distribution of the crystals and the fitted critical percolation exponent.

3.2. Apparent and plastic viscosity

Apparent viscosity – the ratio of measured shear stress to applied shear rate at a specific shear rate – data for suspensions is often characterized by applying the Krieger–Dougherty (K–D) equation [7,22,25]:

$$\eta_r = \frac{\eta_s}{\eta_c} = \left(1 - \frac{\phi}{\phi_m}\right)^{-[\eta]\phi_m} \tag{3}$$

where η_r is the relative viscosity, η_s is the measured viscosity of the suspension, η_c is the viscosity of the continuous phase (pore solution), ϕ is the particle volume fraction, ϕ_m is the maximum (packing)

volume fraction, and $[\eta]$ is the intrinsic viscosity (with a value of 2.5 for rigid spheres [7], but typically a value closer to 6 for cement-based materials [22,25]). In the current experiments, ϕ is constant at 0.472 and two assumptions were employed for the value(s) of $[\eta]$, a constant value of 6 for all mixtures and composite values calculated using $[\eta] = V_{cem}[\eta]_{cem} + V_{FA}[\eta]_{FA}$, where V_{cem} and V_{FA} refer to the volume fractions of cement and fly ash in each mixture ($V_{cem} + V_{FA} = 1$) and $[\eta]_{cem} = 5.25$ and $[\eta]_{FA} = 4.05$ were obtained by fitting the measured apparent viscosities for the first two mortar mixtures (cement only and the original cement/original fly ash blend). The fitted coefficient for fly ash is less than that for cement, as would be expected due to its generally more spherical particle shapes. The $[\eta]$ values were then used along with the maximum packing fractions obtained from the centrifuge experiments (Table 3) to compute the estimated apparent relative viscosities at a shear rate of $25\ s^{-1}$. The centrifuge-measured maximum packing fractions ranged between 0.50 and 0.58 for the mixtures investigated in this study, while those obtained from the spherical particle packing simulations varied between 0.63 and 0.67. The simulation values are likely higher due to the assumption of spherical particles, which typically pack better than irregularly-shaped ones. Fig. 5 provides plots of the K–D computed relative apparent viscosities vs. the measured values for the two assumed values of $[\eta]$. It is clearly observed that the relationship is not one-to-one (R^2 of 0.58 and 0.64 for the fixed and composite values of $[\eta]$, respectively) and that these logical attempts to apply the K–D equation to the current apparent viscosity data set have not succeeded.

Because the yield stress makes a significant contribution to the apparent viscosity computed at a shear rate of $25\ s^{-1}$, the K–D analysis was repeated considering the plastic viscosity values from Table 3 instead. In this case, a value of $[\eta] = 5.5$ was used for the constant case, while the best fit $[\eta]$ values for the composite model were $[\eta]_{cem} = 4.86$ and $[\eta]_{FA} = 4.04$. The agreement between model and measured values shown in Fig. 5 is slightly improved relative to the apparent viscosity analysis, but still, the determined R^2 are only 0.49 and 0.53 for the fixed and composite values of $[\eta]$, respectively. A better fit to the experimental data could perhaps be obtained by adjusting the intrinsic viscosity to be a function of cement and fly ash PSDs, as well as their volume fractions, but there is little justification for doing this in the existing literature [7,22,25].

As summarized recently by Senapati et al. [26], there are a variety of other models in the literature to relate viscosity to particle volume fraction and maximum packing fraction. Two that were evaluated for the current plastic viscosity data set were those of Liu [27] and of Chong et al. [28]. The former fits the relative viscosity data to an equation of the form [27]:
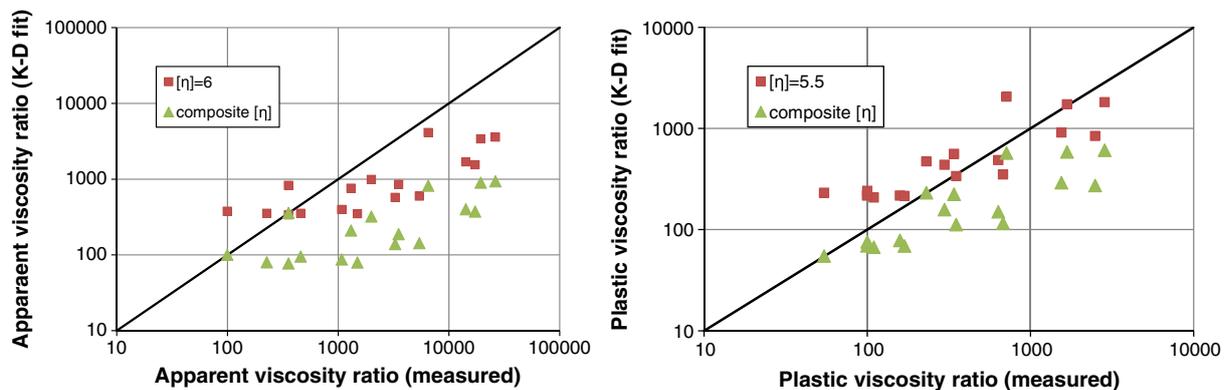
$$\eta_r = [a(\phi_m - \phi)]^{-n} \tag{4}$$

Fig. 5. Apparent (left) and plastic (right) viscosity ratios predicted by applying the K–D equation vs. those measured for the various cement/fly ash mixtures.
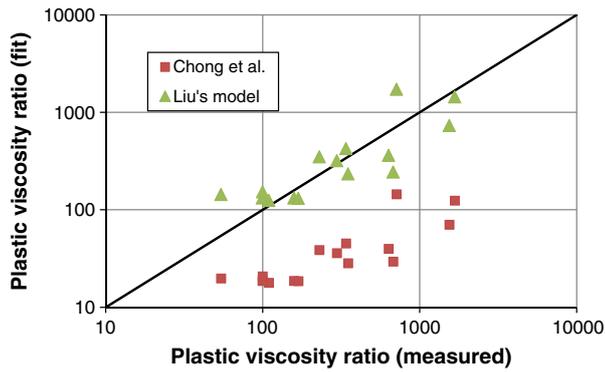
Fig. 6. Plastic viscosity ratios predicted by applying the Liu or Chong et al. equations vs. those measured for the various cement/fly ash mixtures.

Fig. 8. Measured plastic viscosity vs. total particle (number) density. Best fit ($R^2 = 0.792$) is shown for all data with measured viscosities of less than 2 Pa·s.

where a and n are the fitting parameters. The latter also predicts the relative viscosity as a function of particle volume fraction and maximum packing fraction, according to [28]:

$$\eta_r = \{1 + (0.75\phi/\phi_m)/[1-(\phi/\phi_m)]\}^2. \tag{5}$$

For both equations, the value of ϕ_m for each mixture was obtained from analysis of the centrifuging data. The results of applying these two equations to the current data set, for measured plastic viscosities below 2 Pa·s, are provided in Fig. 6. While the model of Chong et al. dramatically underpredicts the measured relative plastic viscosities, that of Liu (with $a = 0.95$ and $n = 2.14$) provides a more reasonable prediction, with $R^2 = 0.70$.

Given the observed limitations of applying these equations to this particular viscosity data set, relationships between plastic viscosity and PSD characteristics were also explored. For measured plastic viscosities below 2 Pa·s (or 15 of the 17 measurable mixes), linear regressions against either total surface area (Fig. 7) or total particle number density (Fig. 8) yielded reasonable correlations. As would be expected, a higher total surface area leads to higher plastic viscosity values. In both cases, these fits were improved relative to considering only the cement particle surface area or the cement particle (number) density, respectively. When a multi-linear regression was conducted with cement surface area and fly ash surface area as independent variables, the fit was not improved and the computed slopes for these two independent variables were within 10% of one another. This suggests that for the plastic viscosity of a flowing system, both the cement and the fly ash particles are contributing to the measured increase relative to the value for the solution itself, in contrast to the yield stress, which was dominated by the properties of the cement particles. It is interesting to note that while the data in references [6] and [7] for the rheological properties of chocolate was not
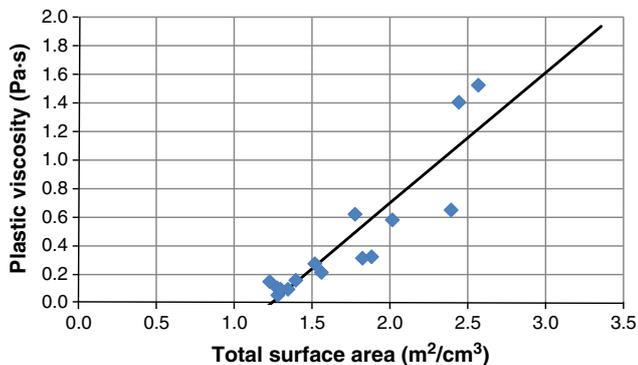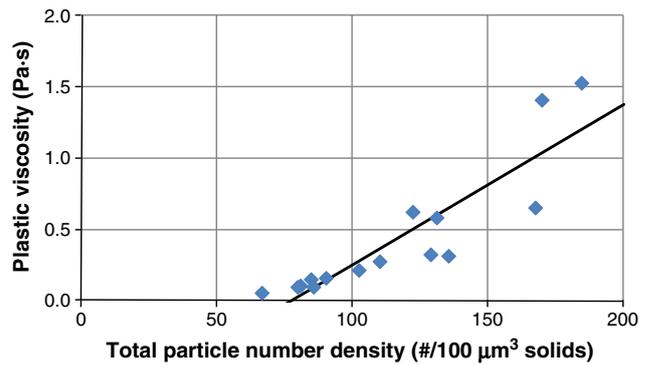
presented in this fashion, data sets from both publications indicate relatively linear monotonic relationships between apparent viscosity and specific surface area.

It must be noted that all mixtures in the current study were intentionally examined without the addition of any water reducers. These chemical admixtures can drastically alter the rheological properties of the pastes, as they typically absorb on the particle surfaces, thus influencing both yield stress and plastic viscosities. For pastes without admixtures prepared using the raw materials examined in this study, one could design a paste with desired values for yield stress and plastic viscosity, by first applying the percolation-type relationship in Eq. (2) to determine an appropriate cement particle density for the desired yield stress and then utilizing either Fig. 7 or Fig. 8 to determine the necessary fly ash characteristics to achieve an appropriate total surface area or total particle density that would yield the desired plastic viscosity value.

4. Conclusions

Both yield stress and viscosity (apparent or plastic) are strongly dependent on the particle characteristics of the powders employed in preparing a blended cement/fly ash paste with a constant volume fraction of water. By measuring the PSDs of both mixture components, it was found that both particle densities and particle surface areas, as determined from these measured PSDs, are critical parameters influencing rheological response. Yield stress is dominated by the particle density of the cement component, with the fly ash mainly acting as a diluent that effectively decreases the cement particle number density. A percolation-type relationship can be employed to relate yield stress to cement particle density in the blended systems. Viscosities are influenced by both cement and fly ash particles, with approximate linear relationships between plastic viscosity values and either total particle surface area or total particle density being found. A quantitative analysis of the relationships between powder particle characteristics and rheological properties allows engineering of the latter via proper selection and control of the former.

Fig. 7. Measured plastic viscosity vs. total surface area. Best fit ($R^2 = 0.817$) is shown for all data with measured viscosities of less than 2 Pa·s.

References

[1] C.F. Ferraris, K.H. Obla, R. Hill, The influence of mineral admixtures on the rheology of cement paste and concrete, Cem. Concr. Res. 31 (2001) 245–255.

[2] A. Papo, L. Piani, R. Ricceri, Rheological properties of very high-strength Portland cement pastes: influence of very effective superplasticizers, Int. J. Chem. Eng. (2010) (2010), doi:10.1155/2010/682914 7 pp.

[3] S.H. Lee, H.J. Kim, E. Sakai, M. Daimon, Effect of particle size distribution of fly ash–cement system on the fluidity of cement pastes, Cem. Concr. Res. 33 (2003) 763–768.

[4] S.D.C. Walsh, M.O. Saar, Magma yield stress and permeability: insights from multiphase percolation theory, J. Volcanol. Geotherm. Res. 177 (2008) 1011–1019.

[5] S.D.C. Walsh, M.O. Saar, Numerical models of stiffness and yield stress growth in crystal-melt suspensions, Earth Planet. Sci. Lett. 267 (2008) 32–44.

[6] E.O. Afoakwa, A. Paterson, M. Fowler, Effects of particle size distribution and composition on rheological properties of dark chocolate, Eur. Food Res. Technol. 226 (2008) 1259–1268.

[7] T.-A.L. Do, J.M. Hargreaves, B. Wolf, J. Hort, J.R. Mitchell, Impact of particle size distribution on rheological and textural properties of chocolate models with reduced fat content, J. Food Sci. 72 (2007) E541–E552.

[8] L.A. Hough, M.F. Islam, P.A. Janmey, A.G. Yodh, Viscoelasticity of single wall carbon nanotube suspensions, Phys. Rev. Lett. 93 (2004), doi:10.1103/PhysRevLett.93.168102.

[9] A. Loiseau, J.F. Tassin, Model nanocomposites based on laponite and poly(ethylene oxide): preparation and rheology, Macromolecules 39 (2006) 9185–9191.

[10] ASTM C150-07, Standard Specification for Portland Cement, ASTM International, 2007.

[11] ASTM C618-08a, Standard Specification for Coal Fly Ash and Raw or Calcined Natural Pozzolan for Use in Concrete, ASTM International, 2008.

[12] ASTM C188-09, Standard Test Method for Density of Hydraulic Cement, ASTM International, 2009.

[13] ASTM C311-07, Standard Test Methods for Sampling and Testing Fly Ash or Natural Pozzolans for Use in Portland-Cement Concrete, ASTM International, 2007.

[14] T.P. Ryan, Modern Experimental Design, Wiley & Sons, Hoboken, 2007.

[15] R.A. Helmuth, L.M. Hills, D.A. Whiting, S. Bhattacharja, Abnormal Concrete Performance in the Presence of Admixtures, 1995 PCA serial # 2006.

[16] G. Sant, C.F. Ferraris, J. Weiss, Rheological properties of cement pastes: a discussion of structure formation and mechanical property development, Cem. Concr. Res. 38 (2008) 1286–1296.

[17] V.A. Hackley, C.F. Ferraris, The use of nomenclature in dispersion science and technology, NIST Recommended Practice Guide, SP 960-3, 2001.

[18] G. Schramm, A practical Approach to Rheology and Rheometry, Haake, 1994.

[19] C.F. Ferraris, M. Geiker, N.S. Martys, N. Muzzatti, Parallel-plate rheometer calibration using oil and lattice Boltzmann simulation, J. Adv. Concr. Technol. 5 (2007) 363–371.

[20] S. Amziane, C.F. Ferraris, Cementitious paste setting using rheological and pressure measurements, ACI Mater. J. 104 (2007) 137–145.

[21] M.A. Galler, A model for settling and packing of tri-axial ellipsoids. Master's thesis, University of Maryland, 2001.

[22] L. Struble, G.-K. Sun, Viscosity of Portland cement paste as a function of concentration, Adv. Cem. Bas. Mater. 2 (1995) 62–69.

[23] D.P. Bentz, Cement hydration: building bridges and dams at the microstructure level, Mater. Struct. 40 (2007) 397–404.

[24] V.M. Malhotra, P.K. Mehta, Pozzolanic and Cementitious Materials, OPA, Amsterdam, 1996.

[25] H. Justnes, H. Vikan, Viscosity of cement slurries as a function of solids content, Ann. Trans. Nordic Rheology Soc. 13 (2005) 75–82.

[26] P.K. Senapati, D. Panda, A. Parida, Predicting viscosity of limestone–water slurry, J. Min. Mater. Char. Eng. 8 (2009) 203–221.

[27] D.M. Liu, Particle packing and rheological property of highly-concentrated ceramic suspensions: ϕ_m determination and viscosity prediction, J. Mater. Sci. 35 (2000) 5503–5507.

[28] J.S. Chong, E.B. Christiansen, A.D. Baer, Rheology of concentrated suspensions, J. Appl. Poly. Sci. 15 (1971) 2007–2021.